Hindawi
Mathematical Problems in Engineering
Volume 2018, Article ID 3252653, 20 pages
https://doi.org/10.1155/2018/3252653

Research Article

Multiple Model Predictive Functional Control for Marine Diesel Engine

Runzhi Wang, Xuemin Li, Yufei Liu, Wenjie Fu, Shuang Liu, and Xiuzhen Ma

College of Power and Energy Engineering, Harbin Engineering University, Harbin 150001, China

Correspondence should be addressed to Xuemin Li; lxm@hrbeu.edu.cn

Received 11 December 2017; Accepted 28 March 2018; Published 14 May 2018

Academic Editor: Xinkai Chen

A novel control scheme based on multiple model predictive functional control (MMPFC) is proposed to solve the cumbersome and time-consuming parameters tuning of the speed controller for a marine diesel engine. It combines the MMPFC with traditional PID algorithm. In each local linearization, a first-order plus time delay (FOPTD) model is adopted to be the approximate submodel. To overcome the model mismatches under the load disturbance conditions, we introduce a method to estimate the open-loop gain of the speed control model, by which the predictive multimodels are modified online. Thus, the adaptation and robustness of the proposed controller can be improved. A cycle-detailed hybrid nonlinear engine model rather than a common used mean value engine model (MVEM) is developed to evaluate the control performance. In such model, the marine engine is treated as a whole system, and the discreteness in torque generation, the working imbalance among different cylinders, and the cycle delays are considered. As a result, more reliable and practical validation can be achieved. Finally, numerical simulation of both steady and dynamic performances of the proposed controller is carried out based on the aforementioned engine model. A conventional well-tuned PID with integral windup scheme is adopted to make a comparison. The results emphasize that the proposed controller is with stable and adaptive ability but without needing complex and tough parameters regulation. Moreover, it has excellent disturbance rejection ability by modifying the predictive multimodels online.

1. Introduction

Diesel engines are the most pervasive and favored prime movers or power sources in the domain of ship for their superior efficiency [1–3]. Speed control is the crucial task for the diesel engines, because the engine performance and service life of the engine and ship rely very much on the speed adjusting [4]. Especially for the diesel engines serving as the marine main engine for propulsion, it is necessary to govern the engine speed during the whole operating processes. Otherwise, the oscillation of engine speed leads to the engine being unable to operate normally [1]. Moreover, the overspeed caused by poor speed governing performance will bring irreversible damage in the marine main engine [5]. It should be pointed out that large speed fluctuation of the engine may cause heavy vibration and strong impact forces, inducing damaging vibration in the related structures leading to premature failure of the transmission system [6]. Hence, the crucial control targets should include (1) tracking the speed set-point quickly and keeping the possible smallest deviations from the desired speed and (2) recovering fast from the external disturbances. According to the practical needs, speed control strategies for the marine diesel engines have drawn considerable attention during the last decades.

However, the speed control algorithm design for the marine diesel engine remains to be a tough mission due to its inherent high nonlinearity. As for the engine speed, it is a function of various aspects, such as the ambient temperature and humidity, fuel injection timing, and compression and combustion processes. And some of these parameters also rely on the transient engine speed to a larger extent at the same time [7]. Furthermore, speed and load of the marine main engine are strongly affected by numerous other external aspects, such as the weather in the sea and the surface condition of the sea [2, 8]. Attempts have been made on the basis of variable control method, such as conventional PID method [9], sliding mode control (SMC) [2], H_∞ control [10],

active disturbance rejection control (ADRC) [11], fuzzy control [5], and model predictive control (MPC) [12].

Although remarkable progress has been acquired, there are still some drawbacks. Specifically, H_∞ control and MPC techniques not only rely on exact mathematical model, but also require high-performance processor to execute the complex matrix computation. As shown in [12], the MPC method was carried out with the help of two 900-MHz IMB PPC processors, which actually cannot be accepted commercially. Despite the fact that there exists computationally efficient MPC algorithm with online linearization and quadratic optimization (e.g., [13–15]), where the online computational requirement is acceptable, such computational simplicity is generally realized by sacrificing the control performance as the linear approximation is invalid when the system state and input deviate far away from where they are linearized. Meanwhile, all these advanced methods still suffer from tiring tuning process [9].

As a result, most of the commercial controllers for marine main engine are based on PID or PI [3, 4, 9]. However, control parameter tuning is still intractable. Hence, the control gains in PID scheme need to be calibrated carefully locally, which is mostly achieved by complicated experiments via trial-and-error approach during various operating conditions, and such process is both costly and time-consuming. Unfortunately, when harsh uncertain external condition causes the operating point of the engine to deviate farther from its calibrated condition, the well-tuned PID controller still cannot guarantee good property [4].

Recently, modern control theory and intelligent control method are applied to improve the adaptive and robust performance of the traditional PID control scheme in marine engine speed control. For instance, a self-turning PID controller based on BP neural network was designed for a large-scale low-speed two-stroke marine diesel engine [16]; better control performance was achieved in simulation. Fuzzy control method was combined with PID to intelligently regulate the parameters of the speed controller online for a MAN B&M type diesel engine. The results showed the proposed fuzzy-PID controller possesses high anti-interference and strong robust abilities [17]. The H_∞ control scheme was utilized as a tuning methodology for the PID speed regulator in [3] to guarantee the robustness against neglected dynamics in a propulsion marine engine and so on.

However, we still underline that the application of MPC method in engine control domain is an unstoppable tendency, various up-to-date relevant articles are giving clue (e.g., [18–21]), and just some issues as mentioned need to be solved furtherly. In many other industrial fields, some researchers started to pay attention to combine PID with MPC. In such applications, the tuning parameters of PID are obtained by MPC optimization law online to keep the advantages and alleviate the shortcomings in both methods. The control performance of these applications has been reported to be excellent. For example, PID was combined with predictive functional control (PFC) [22–25], synthesized with generalized predictive control (GPC) [26, 27], compounded with dynamic matric control (DMC) [28, 29], composited of some other predictive methods as shown in [30, 31].

Up to now, there is no related study published in the field of marine diesel engine yet. Hence, it is deserved to study such kind of application in marine engine speed control, expecting to get good performance and reduce parameters adjustment.

Apart from the above facts, for marine diesel engine speed control, temporally, it is reported that most of the control algorithms were verified via engine models. Some of these models were commonly used mean value engine models (MVEM) [2], and some were even simple low-order transfer function models [3, 32] or another kind of reduced complexity engine model [10]. In such situation, if a model could simulate the characteristics of the engine closer to the real one, it would help to make the verification of control algorithm more reliable and practical. Some innovative examples considered the discrete events in reciprocating engines, and hybrid models (the existence of discrete and continuous model) were studied to model the engine behaviors closer to the reality, such as [33, 34]. However, these models did not consider the whole engine system and only paid attention to intake manifold dynamic and the discrete events in torque generation, and they were merely limited at the idle mode. Some other important characteristics are ignored in such models, such as the working imbalance among different cylinders and the cycle delays, which have a significant effect in engine speed response and can influence the controller's performance. Besides, cylinder-by-cylinder engine model (CCEM) also has been introduced into the engine control domain [35]. Although it can simulate engine more realistically, it requires in-cylinder pressure map, which has higher cost and is difficult to implement [36].

Motivated by the previous research and the challenges stated above, this paper develops a novel control scheme which combines the multiple model predictive functional control (MMPFC) with conventional PID for the marine diesel engine speed control, which markedly simplifies the parameter tuning work. The main contributions of this paper are listed as follows.

First, we adopt the multiple model strategy, which aims at solving the high nonlinearity and various working conditions of the marine diesel engine. With a set of locally linearized predictive models to approximate the nonlinear system, multimodel approach is able to deal with the nonlinear system with wide working range [37, 38]. Second, the PFC theory is introduced to design the optimizer, which guarantees good tracking performance and robustness with fewer requirements in model structure information. Meanwhile, the calculation amount within the PFC is acceptable, so that the processing speed is fast [39]. The proposed controller is developed via combining the PFC with a classical incremental PID. Third, an online identification algorithm is introduced to obtain the open-loop gain, by which system robustness towards mismatched model is enhanced. Fourth, considering the drawbacks in the existing hybrid model and the difficulty to obtain the CCEM, as a compromise, an accurate cycle-detailed hybrid nonlinear engine model is built in this study to evaluate the proposed controller. On the basis of such engine model, simulation results exhibit that the proposed controller with better performances compared with a well-tuned conventional PID dealt with integral windup scheme.

And the online identification algorithm is effective in improving the system robustness under disturbance loads.

The rest of this paper is structured as follows. In Section 2, the combined MMPFC algorithm for engine speed control is described, and the modification method to update the model parameters online is discussed. In Section 3, a cycle-detailed hybrid nonlinear engine model is constructed for verifying the proposed controller, and the comparison between the proposed engine model and the classic MVEM is analyzed. In Section 4, the combined MMPFC method is illustrated in detail to apply in marine diesel engine speed control. And both steady and dynamic performances of the proposed controller are assessed by comparing with a well-tuned PID controller. In Section 5, a conclusion is given to sum up the whole work.

2. Controller Design

2.1. Description of the Predictive Multimodels for Marine Engine Speed Control. In order to design the control algorithm, the predictive multimodels must be obtained in a certain type. For diesel engine speed control, as shown in [40], the relationship between the control input (injection quality) and the system output (engine speed) is high nonlinear. It is difficult to get the accurate physical model, but fortunately there are simplified methods to obtain other types of model.

When engine runs around a certain speed and load condition, as shown in [41–44], the complex engine model can be regarded as simple low-order linear model. The explanation and proof can be found in [44], where the identified result indicates that it is reasonable to adopt the first-order autoregressive (AR) model to represent the speed control modeling in a diesel engine when it works around a specific speed range. In this study, the FOPTD model is adopted as the predictive model in each locally linearized zone, which holds the equivalent structure as the mentioned first-order AR model. Because it captures the process gain (indicates the size and direction of the process variable response to a control move), overall time constant (describes the speed of the response), and effective dead time (states the delay before the response begins) of the process [37]. Furthermore, this kind of model can be identified easily from both simulation and experimental data, generally, from step response data [42].

The working condition of the engine would vary largely as the engine speed and load change. Although the estimation of the load is difficult, it is easy to measure the engine speed. Hence, the zone of local linearization is divided according to the engine speed, and the predictive multimodels of the engine for designing the proposed controller can be written as

$$G_i(s) = \frac{K_i}{T_i s + 1} e^{-\tau_i s}, \tag{1}$$

where $i = 1, 2, \ldots, N$ represents the different speed stage of the target engine under a certain load condition, and the speed range $i \in [n_e^i, n_e^{i+1})$. $G_i(s)$, K_i, T_i, τ_i are the transfer function model between output and the control input, the process gain, the overall time constant, and the effective dead time during the engine speed range i, respectively.

Remark 1. To upgrade model accuracy, the speed stages above should be divided more and cover all the speed ranges. For example, the whole speed range of the target engine is from 800 rpm to 2000 rpm in this study, it can be divided every 100 rpm or 50 rpm during the whole speed range, and the local model can be identified by step speed response in each stage.

Note that the predictive multimodel in a certain speed stage is not unique, because different controller parameters will provide different result. In this study, the model is identified offline by using the data under a conventional PID controller. The parameters of such PID controller are obtained by simple Z-N method. Hence, the engine speed controller can be designed on the basis of the identified models, which describe the basic dynamic for engine speed system in each speed range.

2.2. Multimodel Switching Method. In multimodel predictive control (MMPC), the switching scheduler is necessary to shift the local model (or local controller) for keeping stable transition among different operating conditions [45]. And the design of the switching scheduler directly affects the stability of the close-loop system [38]. In this study, because the predictive multimodels are gained based on the different engine speed stages, a switching method by referring to the present engine speed is proposed.

As mentioned in (1), when the local model of the speed range $i \in [n_e^i, n_e^{i+1})$ is gained, assuming that this local model is the model at the middle speed point $(n_e^i + n_e^{i+1})/2$, then N local models belong to N speed points are obtained. Linear interpolation is applied to calculate the present model parameters based on the N local models by referring to the present engine speed. This can be realized easily by look-up map method.

2.3. Basic Combined MMPFC-PID Controller. For the predictive multimodels (1), ignoring the time delay, (1) can be discretized as follows:

$$\begin{aligned} y_m(k) = {} & \alpha(k-1)\, y_m(k-1) \\ & + K(k-1)\,(1-\alpha(k-1))\, u(k-1), \end{aligned} \tag{2}$$

where $y_m(k)$ is the output of the predictive model at sampling instant k, $\alpha(k-1) = e^{-T_0/T(k-1)}$. $K(k-1)$ and $T(k-1)$ are process gain and time constant calculated by look-up map method from the predictive multimodels at the sampling instant $k-1$. T_0 is the sample and control time.

The predictive output will be conducted based on the control input at sampling instant k, namely, $u(k)$. First, assume that the control input will keep the same within future p (predictive horizon) steps, that is, $u(k+p) = u(k+p-1) = \cdots = u(k)$.

Hence, the output predicted 1 step ahead of the predictive model from data at the sampling instant k which is

$$y_m(k+1 \mid k) = \alpha(k)\, y_m(k) + K(k)(1-\alpha(k))\, u(k). \quad (3)$$

Then the output predicted 2 steps before the predictive model from data at the sampling instant k:

$$\begin{aligned} &y_m(k+2 \mid k) \\ &\quad = \alpha(k)\, y_m(k+1 \mid k) + K(k)(1-\alpha(k))\, u(k+1) \\ &\quad = \alpha(k)\left(\alpha(k)\, y_m(k) + K(k)(1-\alpha(k))\, u(k)\right) \\ &\qquad + K(k)(1-\alpha(k))\, u(k) \\ &\quad = \alpha(k)^2 y_m(k) + K(k)\left(1-\alpha(k)^2\right) u(k). \end{aligned} \quad (4)$$

Similarly, the output predicted p steps ahead of the predictive model from data at the sampling instant k:

$$\begin{aligned} y_m(k+p \mid k) &= \alpha(k)^p y_m(k) \\ &\quad + K(k)\left(1-\alpha(k)^p\right) u(k). \end{aligned} \quad (5)$$

By taking account of the ignored time delay, the corrected output of the predictive model is given as follows:

$$y_{\text{correct}}(k) = y(k) + y_m(k) - y_m(k \mid k - D(k)), \quad (6)$$

where $y(k)$ is the actual output of the plant at the sampling instant k, $y_{\text{correct}}(k)$ is the corrected output of the predictive model at step k, $D(k) = \tau(k)/T_0$, $\tau(k)$ is the time delay calculated by look-up map method from the predictive multimodels at the sampling instant k.

The future reference trajectory $y_r(k+j)$ is set as

$$y_r(k+j) = \beta^j y(k) + \left(1-\beta^j\right) c(k), \quad (7)$$

where β represents the gentle factor of the reference; $c(k)$ is the set-point at the sampling instant k.

Here, cost function J is chosen as

$$J = \sum_{j=1}^{p} \left(y_r(k+j) - \left(y_m(k+j \mid k) + e(k+j)\right)\right)^2, \quad (8)$$

$$e(k+j) = y_{\text{correct}}(k) - y_m(k), \quad (9)$$

where $e(k+j)$ is the error between the corrected output and the output of the predictive model without time delay.

Remark 2. The cost function means getting the optimal solution within the predictive horizon p rather than only at the predicted p step as mentioned in [24].

By combining (5) with (8), J can be written as

$$\begin{aligned} J = \min \sum_{j=1}^{p} &\left(y_r(k+j)\right. \\ &\left. - \left(\alpha(k)^j y_m(k) + K(k)\left(1-\alpha(k)^j\right) u(k) + e(k+j)\right)\right)^2. \end{aligned} \quad (10)$$

When $\partial J/\partial u(k) = 0$, the optimal control input $u^*(k)$ is

$$\begin{aligned} u^*(k) &= \frac{\sum_{j=1}^{p}\left(y_r(k+j) - \left(\alpha(k)^j y_m(k) + e(k+j)\right)\right)}{\sum_{j=1}^{p} K(k)\left(1-\alpha(k)^j\right)}. \end{aligned} \quad (11)$$

Conveniently, the incremental PID controller is proposed as follows:

$$\begin{aligned} u(k) &= u(k-1) + K_P(k)\, e_1(k) \\ &\quad + K_I(k)\left(e_1(k) - e_1(k-1)\right) \\ &\quad + K_D(k)\left(e_1(k) - 2e_1(k-1) + e_1(k-2)\right), \\ e_1(k) &= c(k) - y(k), \end{aligned} \quad (12)$$

where $e_1(k)$ presents the error between reference value and actual output of the plant at the sampling instant k, $K_P(k)$, $K_I(k)$, $K_D(k)$ are PID parameters at the sampling instant k.

The PID controller can be rewritten as

$$u(k) = u(k-1) + \mathbf{w}(k)^T \mathbf{E}(k)\, \mathbf{w}(k), \quad (13)$$

$$\mathbf{w}(k) = \left[w_1(k), w_2(k), w_3(k)\right]^T, \quad (14)$$

$$\mathbf{E}(k) = \left[e_1(k), e_1(k-1), e_1(k-2)\right]^T, \quad (15)$$

$$\begin{aligned} w_1(k) &= K_P(k) + K_I(k) + K_D(k), \\ w_2(k) &= -K_P(k) - 2K_I(k), \\ w_3(k) &= K_D(k). \end{aligned} \quad (16)$$

By solving (11) and (13) we can get $\mathbf{w}(k)$ as

$$\mathbf{w}(k) = \frac{\left(\sum_{j=1}^{p}\left(\left(y_r(k+j) - K(k)\left(1-\alpha(k)^j\right) u(k-1) + \alpha(k)^j y_m(k) + e(k+j)\right)\right)\right)}{\left(\sum_{j=1}^{p} K(k)\left(1-\alpha(k)^j\right) \mathbf{E}^T(k)\, \mathbf{E}(k) + \lambda\right)}. \quad (17)$$

Here, a variable λ is introduced, and thus the denominator will never become zero.

The optimized PID parameters $K_P(k)$, $K_I(k)$, $K_D(k)$ can be calculated through (16), and they are

$$\begin{aligned} K_D(k) &= w_3(k), \\ K_P(k) &= -w_2(k) - 2K_D(k), \\ K_I(k) &= w_1(k) - K_P(k) - K_D(k). \end{aligned} \quad (18)$$

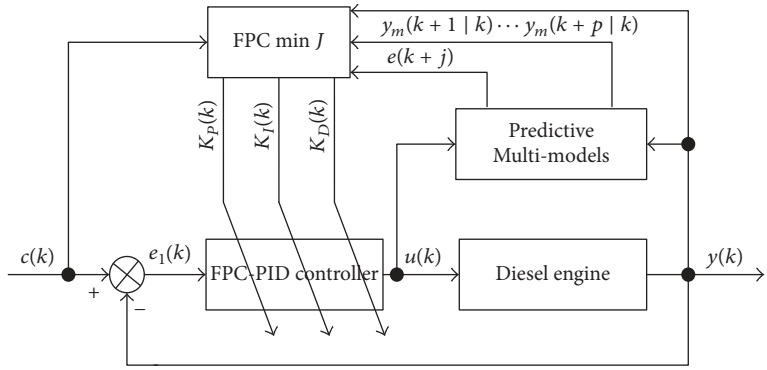

Figure 1: Basic control structure diagram of the MMPFC-PID method.

Here, the PID parameters are optimized by multimodel PFC method. This method can be called MMPFC-PID. And, about the practicability, robustness and stability of the proposed controller can be found similarly in [26]. The basic control structure diagram is illustrated in Figure 1. Provided with proper relative accurate predictive multimodels and basic parameters in the MMPFC-PID method, the proposed controller can optimize the PID parameters in each control step.

2.4. Adaptive Open-Loop Gain Associated MMPFC-PID Controller. Although it has been proved by many previous researchers that the combined PFC-PID controller can keep good performance when the predictive model changes in a certain scale [22–25], it is a fact that the mismatched model would make the control performance deteriorate if the predictive model deviates far from the designed condition [37, 39, 46]. For the marine main engine, the load condition varies more extensively. Particularly, when the wave causes the emergence of the propeller disk from the water, the load of the engine would change violently in such process [47]. Most intuitively, it causes the open-loop gain of the engine speed control modeling to change drastically. The open-loop gain would be far away from its value in the identified condition. In this situation, the basic MMPFC-PID cannot keep good dynamic performance. Hence, the online identification algorithm is necessary for alleviating the influence of model deviation.

In this subsection, the feasible way to estimate the open-loop gain online and its application in MMPFC-PID controller to modify the parameters in FOPTD model will be discussed.

Assume that the diesel engine can be regarded as linear system in each linearized zone. For the linear system, it can be shown by difference equation as follows:

$$y(k) = \alpha_1 y(k-1) + \cdots + \alpha_n y(k-n) + \beta_0 u(k-k_0) + \cdots + \beta_{n-1} u(k-k_0-n+1) + e(k). \tag{19}$$

Select the parameter estimation equation of the object as

$$y(k) = \boldsymbol{\phi}^T(k)\boldsymbol{\theta}(k) + e(k),$$
$$\boldsymbol{\phi}^T(k) = [y(k-1), \ldots, y(k-n), u(k-k_0), \ldots, u(k-k_0-n+1), \widetilde{e}(k-1), \ldots, \widetilde{e}(k-n)],$$
$$\boldsymbol{\theta}^T(k) = [\alpha_1(k), \ldots, \alpha_n(k), \beta_0(k), \ldots, \beta_{n-1}(k), c_1(k), \ldots, c_n(k)], \tag{20}$$

where the estimated residual can be written as

$$\widetilde{e}(k-1) = y(k-1) - \boldsymbol{\phi}^T(k-1)\boldsymbol{\theta}(k-2). \tag{21}$$

The parameters estimation algorithm is given as

$$\boldsymbol{\theta}(k) = \boldsymbol{\theta}(k-1) + \frac{\lambda_1 \boldsymbol{\phi}(k)}{\boldsymbol{\phi}^T(k)\boldsymbol{\phi}(k) + \lambda_2}\left[y(k) - \boldsymbol{\phi}^T(k)\boldsymbol{\theta}(k-1)\right], \tag{22}$$

where λ_1 is the forgotten factor; λ_2 is a constant to avoid the denominator equal to zero.

Then the open-loop gain of the object is estimated by

$$K_\infty = \frac{y(\infty)}{u(\infty)} = \frac{\sum \beta_i}{1 - \sum \alpha_i}, \tag{23}$$

where $y(\infty)$ and $u(\infty)$ mean the system output and control input under steady state, respectively.

Remark 3. This method does not need matrix computation. Hence, it is easy to guarantee convergence and it can be realized easily in engineering perspective. Even though the exact model of the marine main engine is unknown or uncertain, it is possible to estimate the open-loop gain once a relative high-order estimation model is chosen.

Due to the existence of noise in system output and control input, Kalman filter is adopted to dispose the original data to get smooth estimation result.

The process gain in FOPTD model will be replaced by the identified open-loop gain in each control step. Note that although the time constant in FOPTD model for engine speed control modeling cannot be identified easily as the process gain, it has a positive correlation with the process gain in the most conditions. This will be illustrated later in this paper. To simplify the algorithm, the time constant in FOPTD model

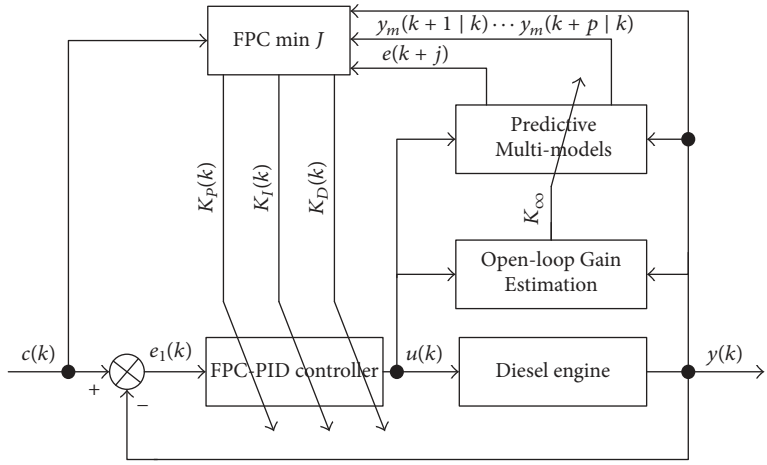

Figure 2: Modified control structure diagram of the MMPFC-PID controller.

can be modified by using the change ratio of the process gain shown as follows:

$$T'(k) = \frac{K_\infty(k)}{K(k)} T(k), \tag{24}$$

where $T'(k)$ means the modified time constant at the sampling instant k, $K_\infty(k)$ is the estimated open-loop gain at the sampling point k, $T(k)$ and $K(k)$ represent the time constant and process gain calculated by look-up map from the predictive multimodels at the sampling instant k.

The basic MMPFC-PID method can be modified with the identification of the open-loop gain online, as shown in Figure 2. It can be called AGMMPFC-PID (adaptive open-loop gain MMPFC-PID) method. When the engine load changes largely, the predictive multimodels can be modified to adapt to the load changing. As a result, the adaptive ability in MMPFC-PID controller can be improved extensively.

3. Engine Model

As mentioned above, a more accurate diesel engine model is necessary for testing the speed control algorithm. In this part, a cycle-detailed hybrid nonlinear engine model which incorporates both discrete and continuous phenomena will be given for the target engine. In such model, the engine is considered as an integrated system. The torque generation is modeled by pulse indicated torque which derives from the MVEM method. Furthermore, the cylinder-by-cylinder variation and the cycle delays are under consideration. The specifications of the target engine are listed in Table 1.

The thermodynamic volumes in the marine diesel engine model are shown in Figure 3. According to the schematic, the engine model consists of five subsystems, namely, intake manifold, exhaust manifold, cylinders, intercooler, and turbocharger.

We will explain the model in two main parts, the discrete-time and continuous-time processes.

Table 1: Target marine diesel engine specifications.

Engine type	Water cooling, inline, 4-stroke, direct injection
Displacement	12.7 L
Number of cylinders	6
Bore/stroke	180/200
Rated power	385 Kw (2000 rpm)
Compression ratio	17.0 : 1
Intake manifold	Turbo charged intercooled

3.1. Discrete-Time Process. To determine the timing sequence of the four strokes in each cylinder during its working cycle, the crank-angle (CA) signal φ is introduced by the integration of the engine speed; that is,

$$\varphi = \mathrm{mod}\left(\int 6n_e dt, 720\right), \tag{25}$$

where n_e is engine speed; operator "mod" represents modulus.

Note that the related position for all the cylinders is steady, for the target engine, 6-cylinder 4-stroke inline engine, the cylinders are distributed on the crankshaft every 120° CA.

For each cylinder, the torque generation mechanism and the in-cylinder evolution process can be illustrated via finite-state machines (FSMs) [33, 34]. As shown in Figure 4, the torque is only generated in the process from "C" to "E." To make use of the advantage of the MVEM method, assuming the torque is kept constant during this process, we substitute the mean torque in the process from "C" to "E" for the mean value in the whole working cycle. Figure 4 also reveals the fact that the intake process and exhaust process happen in a certain timing sequences, which will be used to illustrate the cycle delays later.

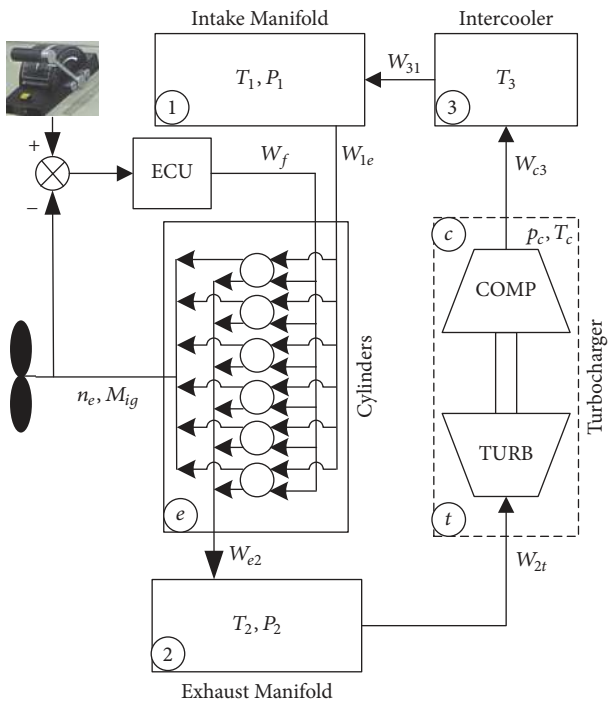

Figure 3: Schematic diagram of the marine diesel engine in a ship for propulsion using. *Note*. W_{ij} denotes the mass flow rate from volume "i" to volume "j." W_f represents the whole mass flow rate injected into the cylinders. T_1 and P_1 are temperature and pressure in intake manifold, respectively. T_2 and P_2 are temperature and pressure in exhaust manifold, respectively. T_3 is the coolant temperature.T_c and P_c are temperature and pressure at the outlet of the compressor, respectively.

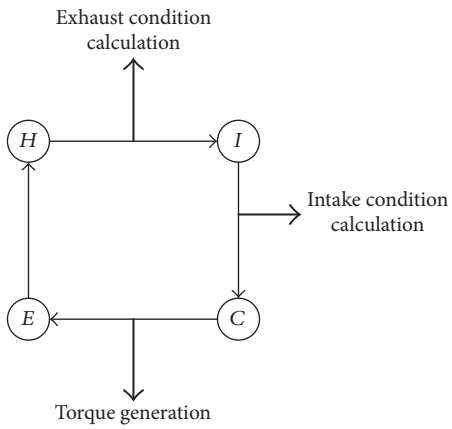

Figure 4: In-cylinder evolution process.

Furthermore, to model the cylinder-by-cylinder variation in cylinders, a factor ξ_i is introduced, which is defined as the cylinder-by-cylinder variation of the cylinder i, requiring $0 \le \xi_i \le 1$, when the gross indicated torque is calculated.

Hence, for the cylinder i, the gross indicated torque M_{ig}^i can be written as

$$M_{ig}^i = P_{\text{durtion}} \frac{30 \cdot W_f^i \cdot q_{HV} \cdot \eta_{ig}^i}{\pi \cdot n_e} \frac{720}{N_c \cdot \varphi_F} \xi_i, \tag{26}$$

$$P_{\text{durtion}} = \begin{cases} 1 & (i-1)\dfrac{360}{N_c} < \varphi < (i-1)\dfrac{360}{N_c} + \varphi_f \\ 0 & \text{otherwise} \end{cases} \tag{27}$$

$$\eta_{ig}^i = f\left(n_e, \lambda^i\right), \tag{28}$$

where P_{durtion} is block pulse function; it makes the gross torque zero except during the expansion phase; as can be explained in (27), W_f^i is the fuel mass flow rate injected into the cylinder i, q_{HV} represents the low calorific value of fuel, η_{ig}^i is the gross indicated efficiency of the cylinder i, it is the function of the engine speed and air to fuel ratio (AFR), and, for the cylinder i, it is λ^i, φ_f is the lasting angle of powering, and for the target engine it is 180° CA, and N_c means the number of total cylinders.

The relationship between W_f^i and the control input m_f (injection quality per stroke per cylinder) is

$$W_f^i = \frac{n_e \cdot N_c \cdot m_f}{120} \cdot 10^{-6}. \tag{29}$$

The total gross indicated torque of all the cylinders M_{ig} is

$$M_{ig} = \sum_1^{N_c} M_{ig}^i. \tag{30}$$

3.2. Continuous-Time Process

3.2.1. Intake Manifold. According to the first law of thermodynamics and the properties of ideal gas, the pressure state equations for intake manifold can be gained as follows:

$$\begin{aligned} \frac{dp_1}{dt} &= \frac{\gamma R}{V_1}\left(W_{c1}T_{c1} - W_{1e}T_1\right), \\ W_{1e} &= \sum_1^{N_c} W_{1e}^i. \end{aligned} \tag{31}$$

The mass flow rate of the intake charger for the individual cylinder i, W_{1e}^i, is

$$W_{1e}^i = \eta_v \cdot \frac{p_1 n_e}{120 R T_1} \cdot \frac{V_d}{N_c}, \tag{32}$$

where η_v is the volumetric efficiency of the engine; V_d is the displacement of the engine.

Note that, in this equation, the value of p_1, n_e, T_1 must be at the moment when W_{1e}^i is calculated, or they cannot donate the mass flow rate of the cylinder i.

3.2.2. Exhaust Manifold. Similar to the intake manifold, the pressure state equations in exhaust manifold can be described as

$$\begin{aligned} \frac{dp_2}{dt} &= \frac{\gamma R}{V_2}\left(W_{e2}T_{e2} - W_{2t}T_2\right), \\ W_{e2} &= \sum_1^{N_c} W_{e2}^i, \\ W_{e2}^i &= W_{1e}^i + W_f^i. \end{aligned} \tag{33}$$

For simplicity, the following assumption is made:

$$W_{1e} = W_{31} = W_{c3}. \tag{34}$$

3.2.3. Intercooler. Ignoring the dynamic in intercooler, the steady state model can be modeled as

$$T_1 = T_c\left(1 - \eta_3\right) + T_3\eta_3, \tag{35}$$

where η_3 means the intercooler efficiency, which can be obtained by experimental data.

The pressure loss in the intercooler is given as

$$\Delta P = P_c - P_1 = k_3\frac{{W_{c3}}^2 RT}{P_c}, \tag{36}$$

where k_3 is the friction factor in the intercooler while the gas is passing by.

3.2.4. Turbocharger. Turbocharger incorporates two components, the turbo and the compressor. Due to the high nonlinearity in turbocharger, it is difficult to derive an accurate physical model. In general, the map based model is adopted by using of the steady state compressor mass flow map and efficiency map, which are related to the turbocharger speed and pressure ratio.

The rotational dynamics of the turbocharger can be written as

$$\frac{dn_t}{dt} = 1000\left(\frac{P_t\eta_m - P_c}{J_t n_t}\right), \tag{37}$$

where n_t is the turbine speed, P_t is the turbine power produced by exhaust, P_c is the power which the compressor consumes, J_t is the inertia, and η_m is mechanical efficiency from turbine to compressor.

P_t can be given as

$$P_t = W_{2t}c_{pe}T_t^*\frac{1}{\eta_t}\left({\pi_t}^{(\gamma_e-1)/\gamma_e} - 1\right), \tag{38}$$

where c_{pe} is the specific heat capacity for exhaust gas at constant pressure, T_t^* is the temperature of the inlet in turbine under stagnation condition, η_t is the turbo efficiency, π_t is the pressure ratio across the turbo, and γ_e is isentropic exponent of exhaust gas.

P_c can be described as

$$P_c = W_{c3}c_{pa}T_c^*\frac{1}{\eta_c}\left({\pi_c}^{(\gamma_a-1)/\gamma_a} - 1\right), \tag{39}$$

where c_{pa} is the specific heat capacity for air at constant pressure, T_c^* is the temperature of the inlet in compressor under stagnation condition, η_c is the compressor efficiency, π_c is the pressure ratio across the compressor, and γ_e is isentropic exponent of air.

The turbo-lag has a large effect during the dynamic process, it can be modeled as a first-order lag. The dynamic of the power demanded by the compressor can be written as

$$\frac{dP_c}{dt} = -\frac{1}{\tau_c}\left(P_t\eta_m - P_c\right), \tag{40}$$

where τ_c is the time constant; for simplicity, we assume it to be a constant.

3.3. Engine Cycle Delays. As shown in Figure 4, the evolution in cylinder happens in different time, which leads to cycle delays of the engine model. These delays can be descripted in either CA domain or the time domain; here we define it in CA domain. We choose the moment at the end of the intake stroke as the reference point. The CA duration of a single stroke is 180° CA for a 4-stroke engine. Through Figure 4, we know that the fuel injection is delayed by 180° CA, and the power stroke relevant variables, such as M_{ig}^i and W_f^i, are delayed by $2 \times 180°$ CA, and the exhaust stroke relevant variables are delayed by $3 \times 180°$ CA. These delays can be realized by setting the updating moments for these related parameters in each cylinder based on the CA domain.

3.4. Load Torque. According to [2, 3] and the references therein, the load torque for a propulsion marine main engine can be normalized and described as

$$M_{\text{load}} = k_{\text{load}}{n_e}^2, \tag{41}$$

where parameter k_{load} represents the integrative effect from the properties of the ship (size, shape, etc.) and the load condition.

The various types of bounded disturbance (disturbances in fuel injection, combustion, load, etc.) are all taken into consideration as M_{noise}, which is gotten by a bounded noise signal.

The load coming from wave is another crucial load disturbance in marine main engine. It can be defined as M_{wave} and simulated via low-frequency sine signal [2, 48].

3.5. Engine Rotational Dynamic Model. Considering the whole effect from the all cylinders, the engine rotational dynamic model can be written as

$$\begin{aligned} J_e\frac{dn_e}{dt} = {} & M_{ig} \\ & - \left(M_p + M_f + M_{\text{load}} + M_{\text{noise}} + M_{\text{wave}}\right), \end{aligned} \tag{42}$$

where J_e is the equivalent rotary inertia for the diesel engine with consideration of its connections (propellers, etc.), M_f is the friction torque, and M_p is the pumping torque.

M_p and M_f can be calculated by the following equations:

$$\begin{aligned} M_p &= \frac{V_d}{4\pi}\left(P_2 - P_1\right), \\ M_f &= \frac{V_d}{4\pi}10^5\left(C_{f1}{n^2}_e + C_{f2}n_e + C_{f3}\right), \end{aligned} \tag{43}$$

where C_{f1}, C_{f2}, C_{f3} are coefficients to decide friction torque, which can be obtained by experiment.

For all the symbols mentioned above, some of them are not annotated; the particular explanation can be found in Figure 3 and the annotation therein.

3.6. Comparison between the Cycle-Detailed Hybrid Nonlinear Engine Model and the MVEM. The comparisons of engine speed responses and indicated torque between the proposed

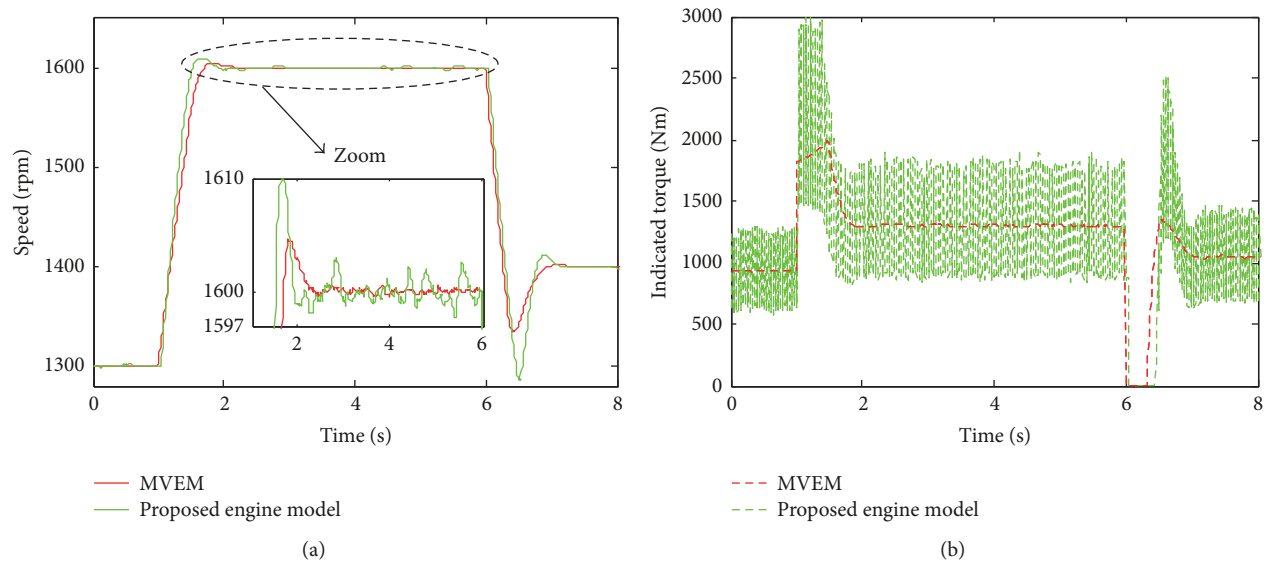

Figure 5: The comparisons of engine models in speed responses (a) and indicated torque (b).

Table 2: The notation for different speed references.

Process	800 rpm to 1200 rpm	1200 rpm to 1600 rpm	1600 rpm to 2000 rpm	2000 rpm to 1600 rpm	1600 rpm to 1200 rpm	1200 rpm to 800 rpm
Notation	I	II	III	IV	V	VI

model and the MVEM are shown in Figure 5. Note that the speed responses in Figure 5 are obtained under the same conditions for both models, which means that the noise load, the load factor, and the parameters of controller are consistent in both cases. As shown in Figure 5(a), more detailed system performance can be observed when the proposed model is adopted. Both the steady and the transient performances in the proposed hybrid nonlinear engine model seem to be inferior to them in the MVEM, because the uncertainties and nonlinearities have been considered more sufficiently in the proposed model. From Figure 5(b), we know that the pulse indicated torque in engine can be shown through the proposed model. Although it is calculated by modified MVEM method as mentioned, it can model the discrete indicated torque without more complex model structure. As we can see, the mean effect of the pulse indicated torque is the same as that in the MVEM (the red dashed line is in the middle position of the green dashed line).

Remark 4. Note that the MVEM was verified in author's previous study [2]. In Figure 5(a), we know that the speed responses between the two models are the same broadly; this also can be regarded as the verification of the proposed model. Limited by the space, here we do not discuss more about it; for more details refer to [2].

To sum up the diesel engine model from the perspective of control, the engine rotational dynamic model (42) can be rewritten in the form of state space:

Table 3: The notation for different load conditions.

Load condition	$k_{\text{load}} = 0.00025$	$k_{\text{load}} = 0.00015$	$k_{\text{load}} = 0.00035$
Notation	Case 1	Case 2	Case 3

$$\begin{aligned} \dot{x} &= f(x,u)\,x + g(x,u)\,u + \omega, \\ y &= x, \end{aligned} \tag{44}$$

where $x = n_e$ is the state variable, control input $u = m_f$, system output y means the engine speed, and ω represents the additive disturbance, primarily including model uncertainties and unmodeled dynamics.

4. Simulation Experiments and Results

In this section, the simulation experiments will be designed based on the proposed engine model.

To compare the system performance for the MMPFC-PID controller and the PID controller in a wide engine working range, the reference speed is decided to include a series of step functions to cover the engine speed range from 800 rpm to 2000 rpm. Specifically, as shown in Table 2, initiate from the idle speed at 800 rpm to the rated speed 2000 rpm; both acceleration (marked as I, II, and III) and deceleration (marked as IV, V, and VI) processes are set.

The three load factors are considered as shown in Table 3; the load factor k_{load} is designed to be 0.00025 in Case 1, and

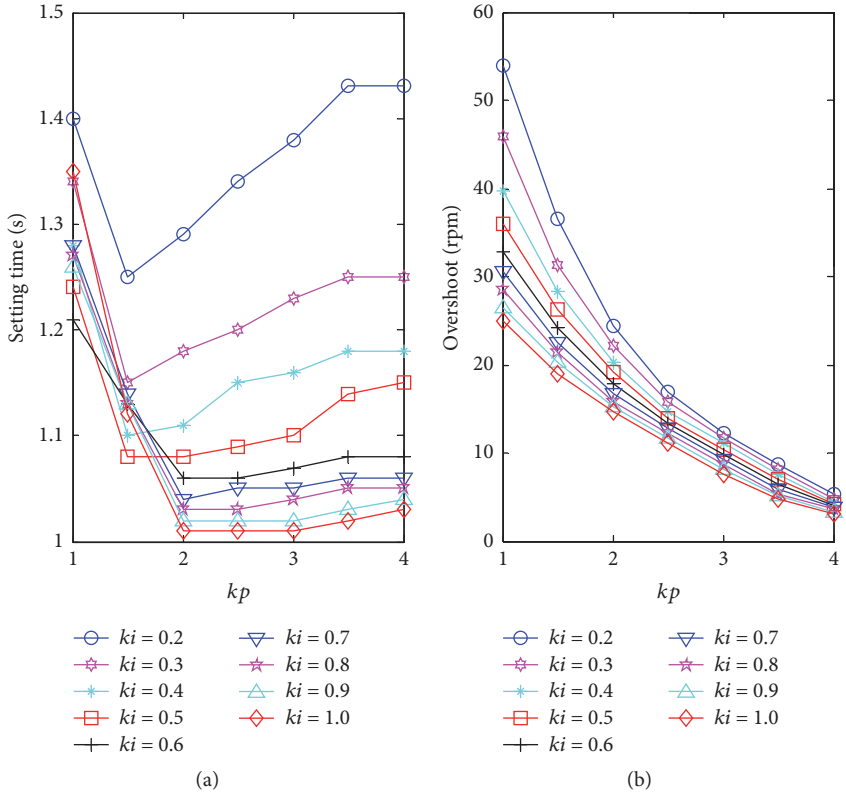

FIGURE 6: The demonstration of tuning PID parameters and the effects of kp and ki on setting time (a) and on overshoot (b).

when it has a deviation of −40% and +40%, Case 2 (k_{load} = 0.00015) and Case 3 (k_{load} = 0.00035) are obtained. The considered load cases cover a wide range of external load.

Both controllers are tested with the mentioned different reference speed signals in each load case to cover the engine operating range extensively.

The control performance comparisons of both controllers in these designed cases are carried out by comparing the indices in setting time (t_s), overshoot percentage (M_p), steady state speed fluctuation ($|\Delta n_e|$), integral absolute error (IAE), and time-multiplied absolute error (ITAE).

Furthermore, the capacity of resisting disturbance for the proposed controller should be evaluated. We choose the 2000 rpm case to execute such test, where the engine is the rated condition and the output power is the maximum. And the disturbance load incorporates two main types, that is, wave load and the mutation load.

4.1. Parameters Design of Controllers

4.1.1. Parameters Design of PID Controller. Because of the nonlinearity and the various working ranges in marine diesel engine, one set of PID parameters cannot keep good performances at different speed stages, different load conditions, and different processes (acceleration and deceleration). Hence, the PID parameters are tuned under Case 1 (regarded as the standard condition) at normal used high-speed condition (between 1600 rpm and 2000 rpm). In such condition, the PID parameters are optimized via trial-and-error approach and deal with integral windup scheme.

Figure 6 demonstrates the effects of basic PID parameters on the performance in setting time and overshoot. There is a trade-off relationship between setting time and overshoot while the proportionality coefficient (kp) is in a reasonable range (from 2 to 4, as shown in Figure 6(a)). When the proportionality coefficient and integral coefficient (ki) vary in the range from 3 to 4 and from 0.5 to 1.0, respectively, a proper performance can be obtained. At the same time, it also needs to make a compromise in the performances among acceleration, deceleration, and steady state processes. Furthermore, it is necessary to take the effect of differential coefficient (kd) into account. Finally, the PID parameters are decided as kp = 3.6, ki = 0.7, and kd = 0.4. From the optimization process above, we know that it is tiring and difficult.

4.1.2. Parameters Design of MMPFC-PID Controller. As for the proposed MMPFC-PID controller, the parameters also are designed under Case 1. To gain the basic input/output (injection quality/engine speed) data for the identification purpose, a closed-loop controller is required [44], because diesel engine is open-loop marginally stable [7, 49]. The closed-loop controller is chosen to be the PID with simple parameters by Z-N approach. With the help of such controller, the input/output data is obtained by setting the engine

Table 4: The parameters of the identified predictive multimodels.

Model parameters	Speed (rpm)											
	850	950	1050	1150	1250	1350	1450	1550	1650	1750	1850	1950
T_i	2.78	2.65	2.67	2.47	2.40	2.26	2.10	2.23	2.00	2.19	2.19	1.44
K_i	16.39	16.12	15.79	15.42	14.95	14.41	13.92	13.31	11.37	12.05	11.51	10.93
τ_i	0.081	0.075	0.071	0.068	0.063	0.058	0.055	0.045	0.041	0.033	0.024	0.015

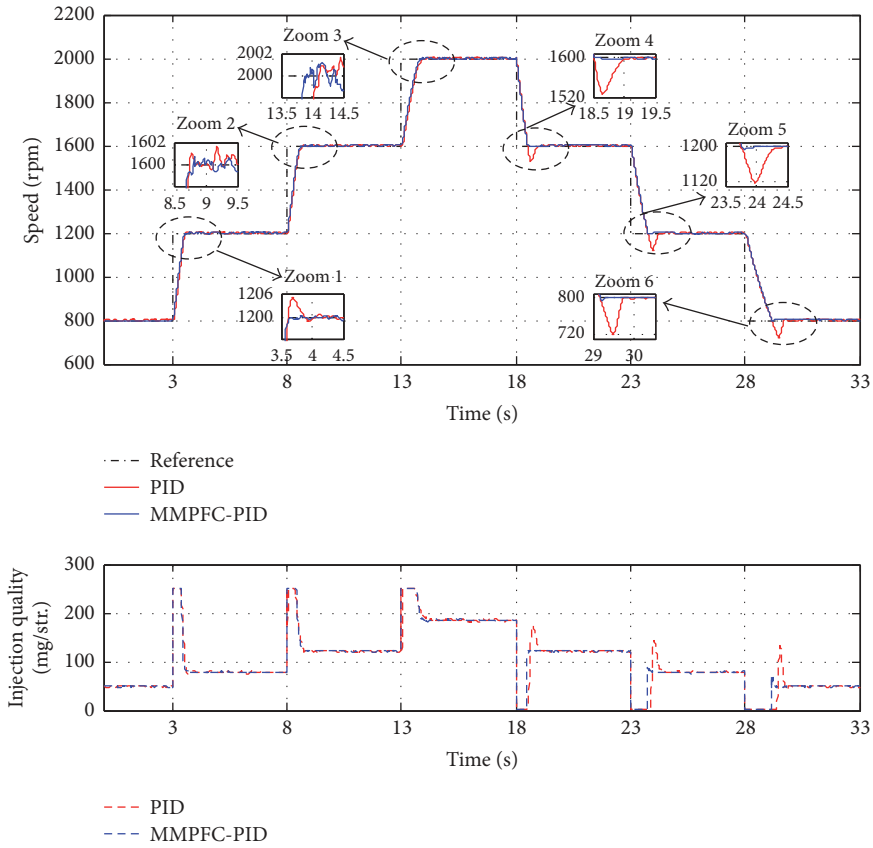

Figure 7: Step speed responses and the control input in Case 1.

speed with step response every 100 rpm between 800 rpm and 2000 rpm.

According to the front contents, the identified predictive multimodels can be shown in Table 4. In general, there is a positive correction between the process gain and the time constant. It provides a way to understand the modification method of the time constant in previous section.

Other parameters for the MMPFC-PID controller are designed as follows: $\beta = 0$, $\lambda = 1$. The predictive horizon p affects the dynamic performance of the MMPFC-PID controller, which implies that a balance between the stability and dynamic response should be considered when we design p. We decide it to be changed with the variation of the time delay, $p = D(k) + 10$. Note that the smooth factor β is designed to be 0 for getting an equitable comparison to the conventional PID controller, as when $\beta = 0$ it means the set-point does not deal with smoothing method and can get the fastest response. And both controllers are with the same sample and control time, $T_0 = 0.01$ s.

4.1.3. Parameters Design of AGMMPFC-PID Controller. As for the AGMMPFC-PID controller, the basic parameters are the same as those in the MMPFC-PID. And the parameters in open-loop gain estimation process are designed as follows: the order of the engine system is chosen to be 3, forgotten factor is set as $\lambda_1 = 0.95$, and constant $\lambda_2 = 0.5$.

4.2. Simulation and Analysis

4.2.1. Speed Tracking Performance under Step Response Conditions. The responses of the engine speed and the corresponding control input for the mentioned Case 1, Case 2, and Case 3 are shown in Figures 7, 8, and 9, respectively. The according performance comparisons for both controllers

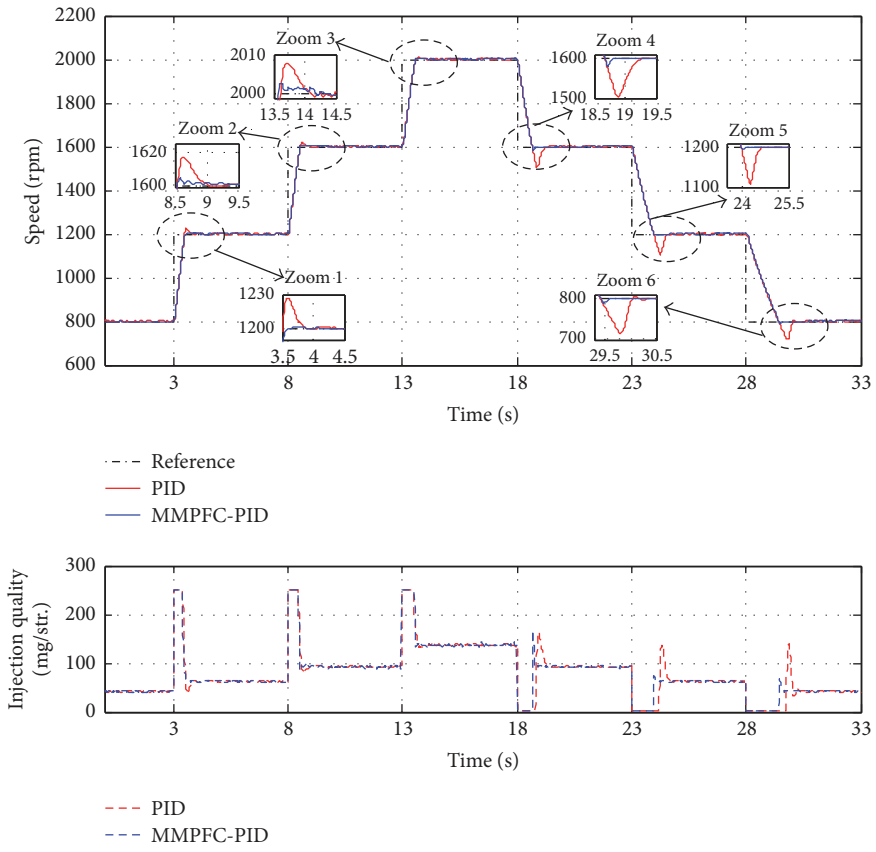

Figure 8: Step speed responses and the control input in Case 2.

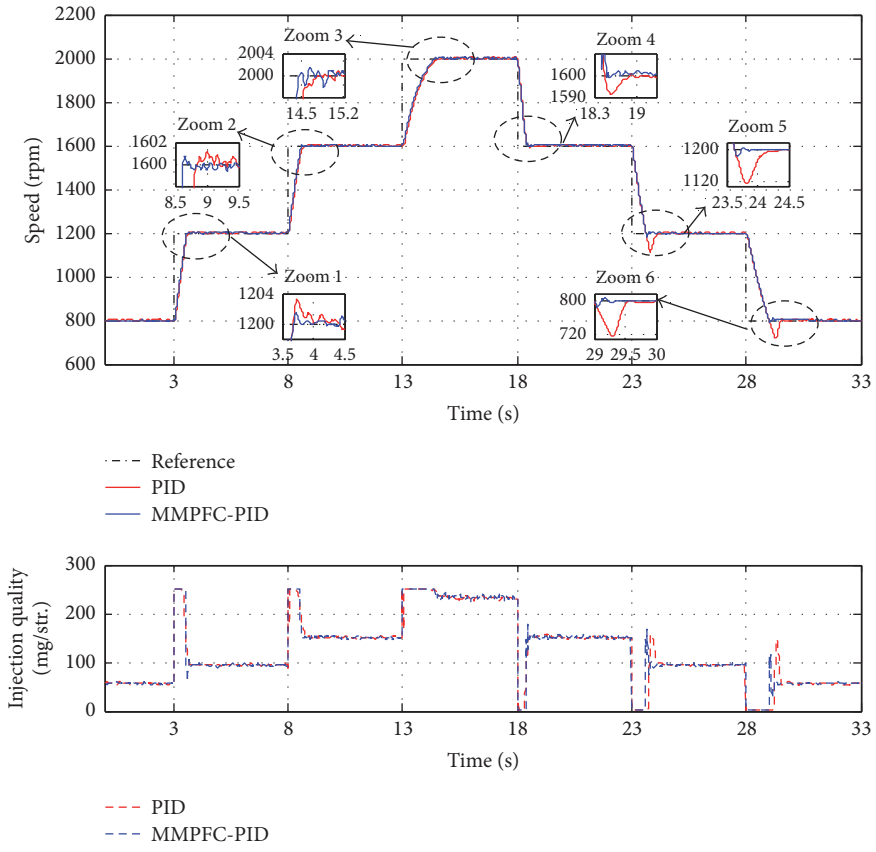

Figure 9: Step speed responses and the control input in Case 3.

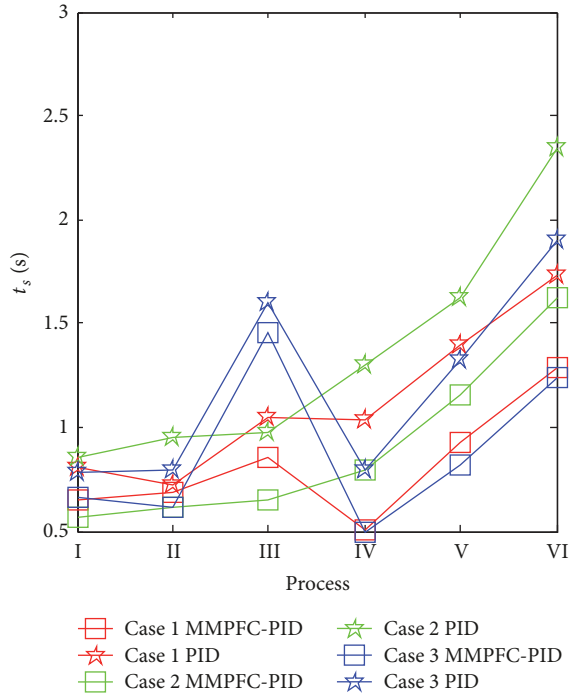

Figure 10: Comparisons of speed tracking performance in the index of setting time (t_s) for all the tested processes and load factors.

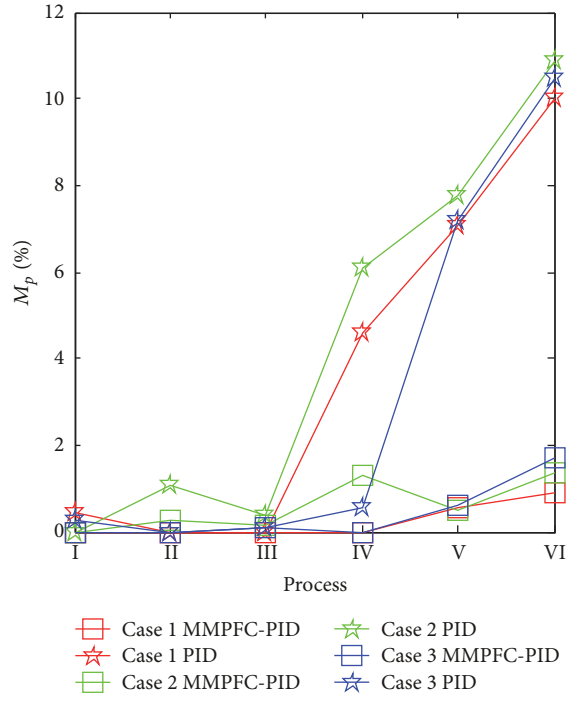

Figure 11: Comparisons of speed tracking performance in the index of overshoot percentage (M_p) for all the tested processes and load factors.

in the criteria of setting time (t_s), overshoot percentage (M_p), steady state speed fluctuation ($|\Delta n_e|$), integral absolute error (IAE), and time-multiplied absolute error (ITAE) are illustrated in Figures 10, 11, 12, 13, and 14, respectively.

In Case 1 (shown in Figure 7), the most apparent trait is that the conventional PID controller cannot provide good performance in reducing overshoot percentage during the deceleration processes (Figure 7: Zoom 4, Zoom 5, and Zoom 6). Detailed information can be found in Figure 11. Although the PID controller is well-tuned in the process IV, the overshoot percentage is still more than 4% (shown in Figure 10, the red line marked with stars). Besides, the

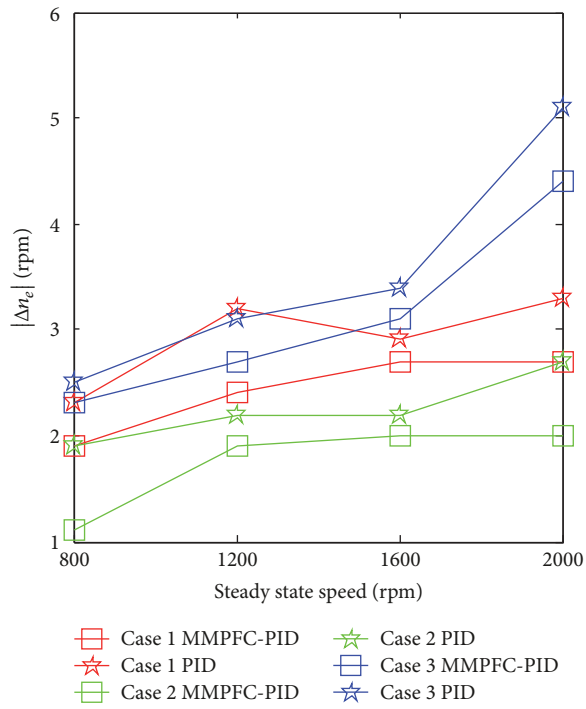

Figure 12: Comparisons of speed tracking performance in the index of steady state speed fluctuation ($|\Delta n_e|$) for all the tested processes and load factors.

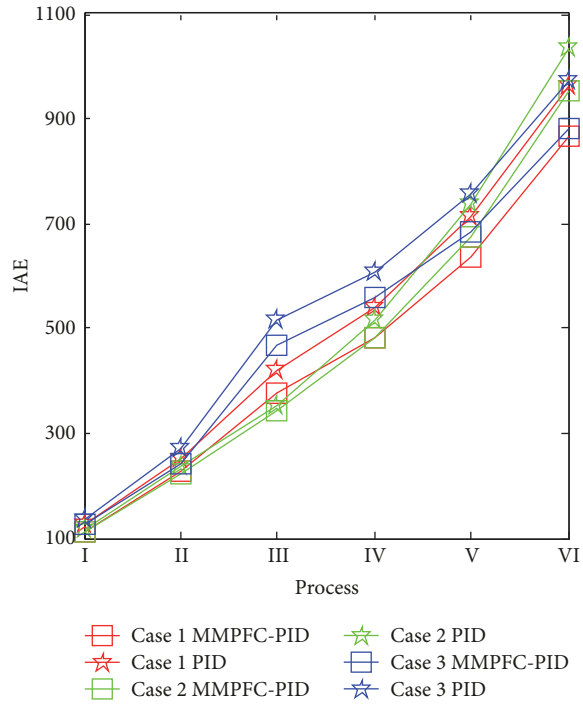

Figure 13: Comparisons of speed tracking performance in the index of integral absolute error (IAE) for all the tested processes and load factors.

overshoot percentages are about 7% and 10% in the processes V and VI (shown in Figure 11, the red line marked with stars).

On the contrary, in the MMPFC-PID controller, the overshoot percentage values are kept less than 1% or even zero in all the acceleration and deceleration processes (shown in Figure 11, the red line marked with squares).

The preponderance in restricting overshoot for the MMPFC-PID controller as mentioned in Case 1 is still

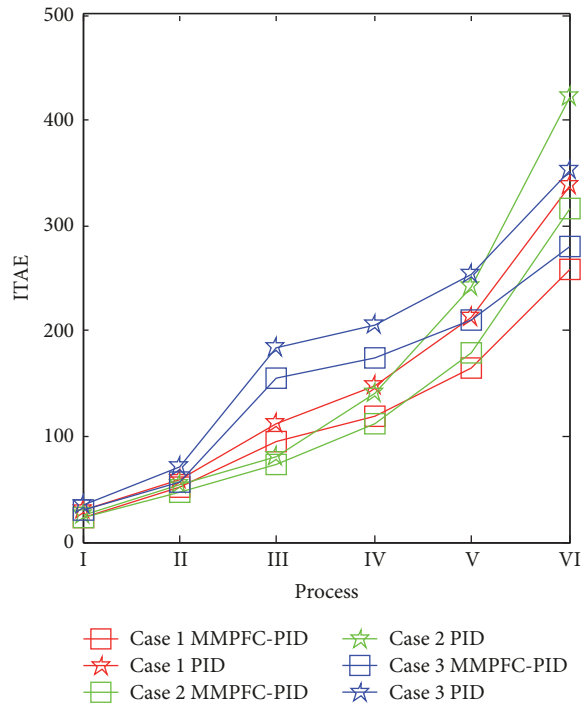

Figure 14: Comparisons of speed tracking performance in the index of time-multiplied absolute error (ITAE) for all the tested processes and load factors.

inherited when it comes to Case 2 and Case 3. Although the load factors vary ±40%, the overshoot percentages in all the processes are kept less than 2% (shown in Figure 11, green and blue lines marked with squares). But for PID, in Case 2 (shown in Figure 8), the overshoot percentages get worse, which are around 6%, 8%, and 11% in the processes IV, V, and VI (shown in Figure 11, green line marked with stars), respectively; in Case 3 (shown in Figure 9), the overshoot percentages are still inferior to them in the MMPFC-PID; they are almost 7% and 10.5% in processes V and VI (shown in Figure 11, blue line marked with stars), separately.

Furthermore, as the indices in steady state speed fluctuation and time-multiplied absolute error can indicate the steady state traits and the indices in setting time and integral absolute error represent the dynamic characteristics [50], it is can be observed from Figures 10, 12, 13, and 14 that the same color lines marked with squares are clearly below the lines marked with stars. Hence, it is evident that the MMPFC-PID controller has better steady and dynamic performances in all the tested processes.

According to the analysis above, the proposed MMPFC-PID controller has better adaptive ability than the conventional well-tuned PID. It also can be deduced from the control input (injection quality) curves, shown in Figures 7–9, that the control input in the proposed controller is adjusted more quickly. It is because the PID parameters in the proposed controller are optimized by multimodel PFC method in each control step rather than keeping the same values in the well-tuned PID controller.

It should be noted that the parameters variations of the proposed controller are not given in this study, because they are totally dynamic optimization processes without a strong regularity. They were also never illustrated in the similar applications in other different fields [22–25, 27].

Table 5: Performance Comparisons under wave load.

Index	Controller		
	AGMMPFC-PID	MMPFC-PID	PID
IAE	70.07	106.52	113.90
$\lvert\Delta n_e\rvert$ (rpm)	5.4	6.2	6.8

4.2.2. Speed Governing Performance under Disturbance Load Conditions. The overall speed responses of the marine diesel engine under the wave load and mutation load conditions are exhibited in Figure 15. The system performance in different disturbance loads are enlarged in Figure 16.

The detailed load changing is shown in Figure 17(a). During the time from 0 s to 10 s, the engine is working under 100% propulsion load condition and the same time disturbed by wave load. From 10 s to 15 s, both propulsion load and wave load are removed totally, but the noise load is kept. And in the last 5 s the total propulsion load and wave load are added in again.

As shown in Figure 16(a), under wave load disturbance situation, the response of the AGMMPFC-PID is better than the performance given by the MMPFC-PID and PID. More details are shown in Table 5. The AGMMPFC-PID method has the smallest values in steady state speed fluctuation

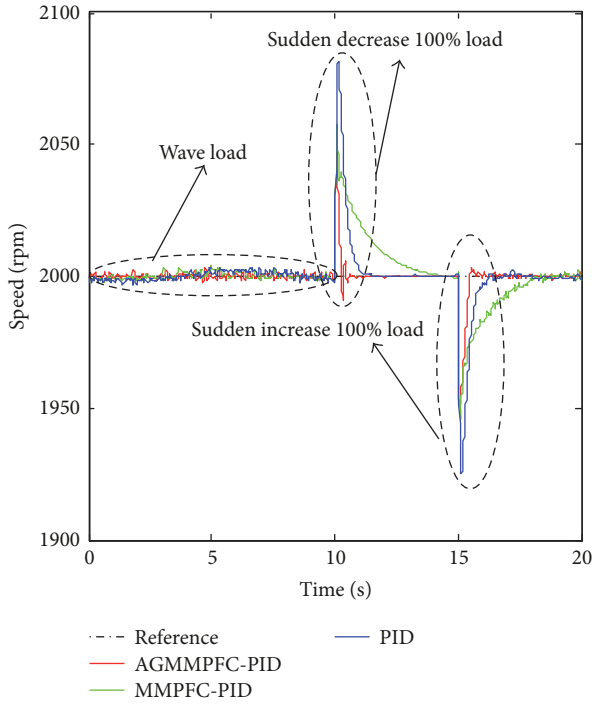

Figure 15: The overall engine speed response in disturbance loads.

Table 6: Performance comparisons under mutation loads.

Index	Controller		
	AGMMPFC-PID	MMPFC-PID	PID
Speed variation (abs. rpm)	46.7[1] 49.1[2]	57.4[1] 54.0[2]	81.0[1] 75.3[2]
Recovery time (s)	0.65[1] 0.70[2]	3.00[1] 2.52[2]	1.40[1] 1.35[2]

Note. 1 means the sudden decrease of 100% load process, 2 means the sudden increase of 100% load process.

($|\Delta n_e|$) and integral absolute error (IAE), they are 5.4 rpm and 70.07, followed by the MMPFC-PID and PID. It indicates that by introducing the open-loop gain in the AGMMPFC-PID to modify the predictive multimodels the fluctuation of engine speed is reduced significantly. It also proves that, even without the model modifying in the MMPFC-PID controller, it still can keep stable and sustain better performance than in the well-tuned PID, but without the same complex parameters adjusting process.

The speed responses of sudden decrease 100% load and sudden increase 100% load conditions are shown in Figures 16(b) and 16(c), respectively. The detailed performance indices are given in Table 6.

From Figures 16(b) and 16(c) and Table 6, we know that the absolute engine speed variations in the original MMPFC-PID are around 40% less than those in the PID case, but recovery time values are longer. From Figure 17(c), we observe that the model mismatch would be very serious under the mutation load conditions: the open-loop gain under the full load condition is about eight, but when without load it becomes around fifty; it means the process gain in the predictive multimodels would change more than six times. It indicates that the MMPFC-PID still has a good closed-loop stability and can keep an acceptable performance when predictive multimodels deviate largely.

Moreover, with the parameters updating in predictive multimodels by identifying the open-loop gain online, the performances of the AGMMPFC-PID in criteria of absolute engine speed variation and recovery time have been improved to be further better than those in the MMPFC-PID and PID during the sudden load changing processes.

By analyzing the response curves of load (Figure 17(a)), control input (Figure 17(b)), and the identified open-loop gain (Figure 17(c)), it is easy to understand that the estimated open-loop gain can properly reflect the load changing in time. It can modify the predictive multimodels online; thus the parameters in PID controller can be optimized by the multimodel PFC method in each control step. As a result, the control input can be regulated faster to restrict the disturbances.

5. Conclusion

To upgrade speed tracking accuracy and enhance disturbance suppression ability for the marine main engine, a novel method is proposed by combining the MMPC theory with PID algorithm, which reduces parameters regulation as well. In this method, the receding-horizon optimization process

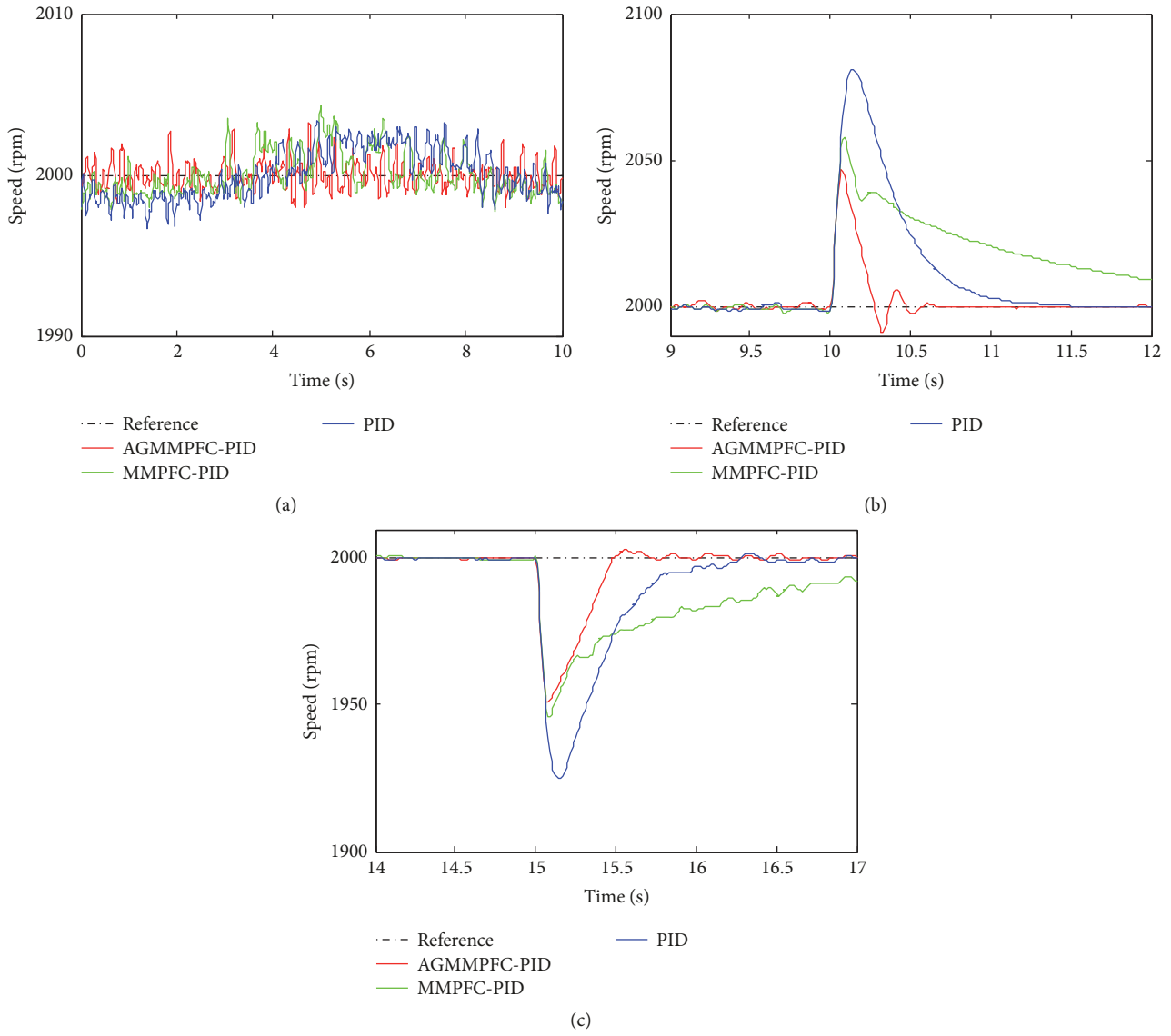

Figure 16: Detailed engine speed responses in wave load (a), sudden decrease of 100% load (b), and sudden increase of 100% load (c).

is carried out based on the MMPFC scheme. To alleviate the model mismatch when load disturbances occur, the estimation of the open-loop gain is adopted to modify the predictive multimodels online.

Meanwhile, a cycle-detailed hybrid nonlinear engine model is established to test the proposed controllers. The simulation experiments demonstrate the following:

(1) The MMPFC-PID controller has more adaptive ability than the well-tuned PID in keeping better steady and transient performance under different propulsion load factors during the whole speed range.

(2) The MMPFC-PID controller is capable of guaranteeing system stability when the disturbance loads cause the predictive model to deviate largely from the designed condition.

(3) Considering the wave disturbance, system performance under the MMPFC-PID controller is better than that in the well-tuned PID. However, the MMPFC-PID controller does not need difficult parameters adjusting process. Under the mutation load conditions, the MMPFC-PID has fewer speed variations but longer setting time compared with the well-tuned PID.

(4) By estimating the open-loop gain and modifying the predictive multimodels online, the AGMMPFC-PID controller obtains better performance than the MMPFC-PID and well-tuned PID controllers in the sense of overcoming wave load and mutation load disturbances.

Conflicts of Interest

The authors do not have any conflicts of interest.

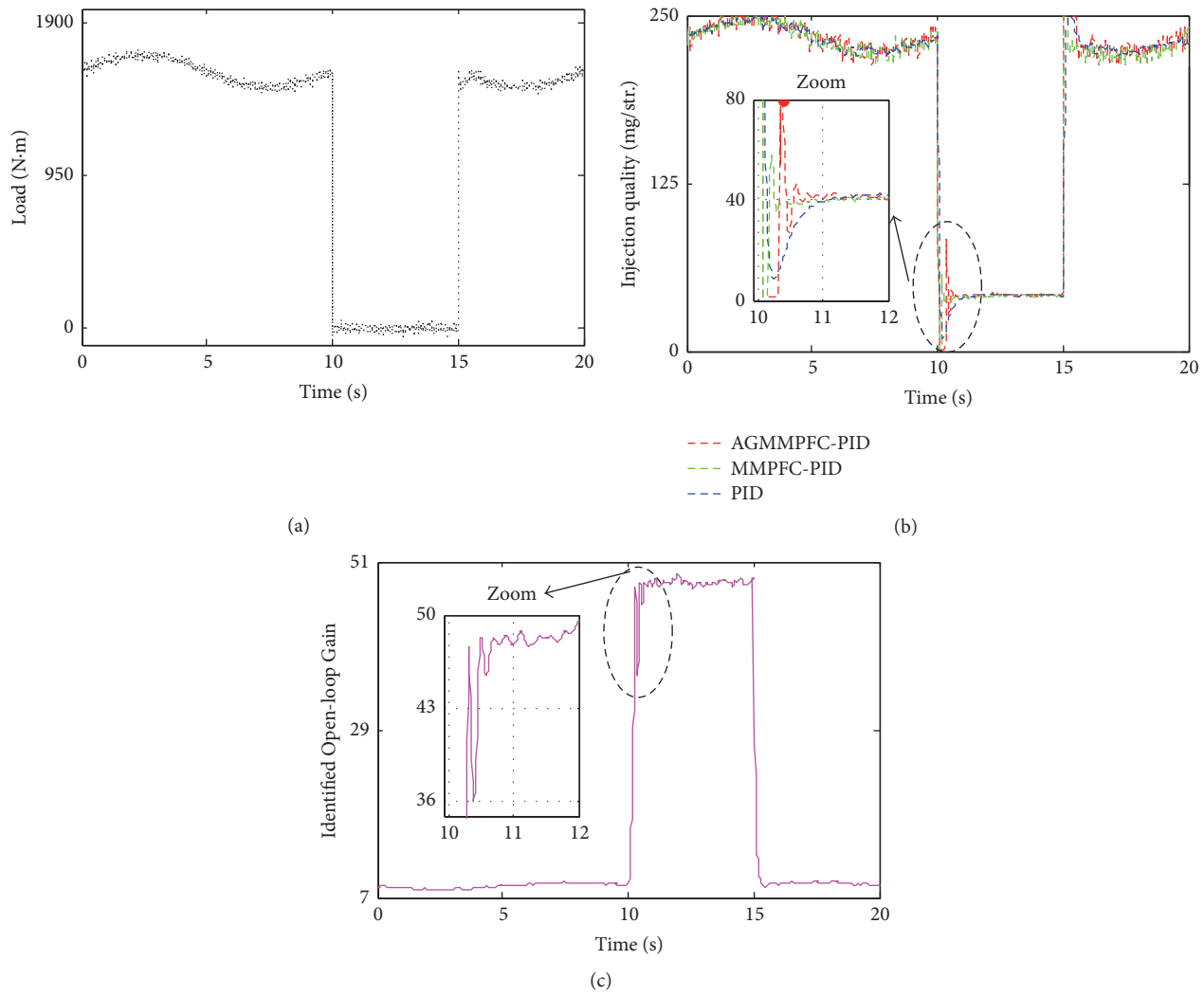

FIGURE 17: The demonstration of the load changing (a), control input changing (b), and identified open-loop gain changing (c) in disturbance loads.

References

[1] Y. Guo, W. Li, S. Yu et al., "Diesel engine torsional vibration control coupling with speed control system," *Mechanical Systems and Signal Processing*, vol. 94, pp. 1–13, 2017.

[2] X. Li, Q. Ahmed, and G. Rizzoni, "Nonlinear robust control of marine diesel engine," *Journal of Marine Engineering Technology*, vol. 16, no. 1, pp. 10–2017, 2017.

[3] N. I. Xiros, "PID marine engine speed regulation under full load conditions for sensitivity H∞-norm specifications against propeller disturbance," *Journal of Marine Engineering and Technology*, vol. 3, no. 2, pp. 3–11, 2004.

[4] P. Weigang, X. Hairong, H. Yaozhen, W. Changshun, and Y. Guiyong, "Nonlinear active disturbance rejection controller research of main engine for ship," in *Proceedings of the 2010 8th World Congress on Intelligent Control and Automation*, pp. 4978–4981, 2010.

[5] C. Lynch, H. Hagras, and V. Callaghan, "Using uncertainty bounds in the design of an embedded real-time type-2 neuro-fuzzy speed controller for marine diesel engines," in *Proceedings of the IEEE International Conference on Fuzzy Systems*, pp. 1446–1453, Vancouver, Canada, July 2006.

[6] J. Wei, A. Zhang, D. Qin et al., "A coupling dynamics analysis method for a multistage planetary gear system," *Mechanism and Machine Theory*, vol. 110, pp. 27–49, 2017.

[7] J. Jiang, "Optimal Gain Scheduling Controller for a Diesel Engine," *IEEE Control Systems Magazine*, vol. 14, no. 4, pp. 42–48, 1994.

[8] L. Haifeng and Lihui, "The speed control of marine main engine," in *Proceedings of the 2014 Sixth International Conference on Measuring Technology and Mechatronics Automation*, pp. 770–773, 2014.

[9] S.-H. Lee, J.-S. Yim, J.-H. Lee, and S.-K. Sul, "Design of speed control loop of a variable speed diesel engine generator by electric governor," in *Proceedings of the 2008 IEEE Industry Applications Society Annual Meeting, IAS'08*, October 2008.

[10] G. Papalambrou and N. P. Kyrtatos, "H∞ robust control of marine diesel engine equipped with power-intake-in system," *IFAC Proceedings Volumes*, vol. 39, no. 12, pp. 591–596, 2006.

[11] H.-D. Hua, N. Ma, J. Ma, and X.-Y. Zhu, "Robust intelligent control design for marine diesel engine," *Journal of Shanghai Jiaotong University (Science)*, vol. 18, no. 6, pp. 660–666, 2013.

[12] T. Broomhead, C. Manzie, P. Hield, R. Shekhar, and M. Brear, "Economic model predictive control and applications for diesel generators," *IEEE Transactions on Control Systems Technology*, vol. 25, no. 2, pp. 388–400, 2017.

[13] A. Zheng, "A computationally efficient nonlinear MPC algorithm," in *Proceedings of 16th American CONTROL Conference*, pp. 1623–1627 vol.3, Albuquerque, NM, USA, June 1997.

[14] F. Martinsen, L. T. Biegler, and B. A. Foss, "A new optimization algorithm with application to nonlinear MPC," *Journal of Process Control*, vol. 14, no. 8, pp. 853–865, 2004.

[15] H. Nguyen Tuan, I. Ismai, N. B. Saad, A. Faisa, and M. Irfan, "A practical approach of control of real time nonlinear process plant using multiple model predictive control," in *Proceedings of the 6th International Conference on Modelling, Identification & Control (ICMIC)*, pp. 59–64, 2014.

[16] W. Meng and C. Guo, "Research on speed intelligent control based on neural networks for large marine main diesel engine," in *Proceedings of the 2010 8th World Congress on Intelligent Control and Automation, WCICA 2010*, pp. 4667–4670, July 2010.

[17] X. Shen and Y. Su, "Marine diesel engine speed control system based on fuzzy-PID," *Applied Mechanics and Materials*, vol. 152-154, pp. 1589–1594, 2012.

[18] Y. Hu, H. Chen, P. Wang, H. Chen, and L. Ren, "Nonlinear model predictive controller design based on learning model for turbocharged gasoline engine of passenger vehicle," *Mechanical Systems and Signal Processing*, vol. 109, pp. 74–88, 2018.

[19] Q. Zhu, R. Prucka, M. Prucka, and H. Dourra, "Model Predictive Engine Speed Control for Transmissions with Dog Clutches," *Journal of Engineering for Gas Turbines and Power*, vol. 139, no. 11, Article ID 112803, 2017.

[20] L. Wei, F. Yan, J. Hu, G. Xi, B. Liu, and J. Zeng, "Nox conversion efficiency optimization based on NSGA-II and state-feedback nonlinear model predictive control of selective catalytic reduction system in diesel engine," *Applied Energy*, vol. 206, pp. 959–971, 2017.

[21] M. E. Emekli and B. Aksun Guvenc, "Explicit MIMO model predictive boost pressure control of a two-stage turbocharged diesel engine," *IEEE Transactions on Control Systems Technology*, vol. 25, no. 2, pp. 521–534, 2017.

[22] H. Li and J. Zhang, "Improved PID design using new state space predictive functional control optimization based structure," *Chemometrics and Intelligent Laboratory Systems*, vol. 151, pp. 95–102, 2016.

[23] S. Wu, "State space predictive functional control optimization based new PID design for multivariable processes," *Chemometrics and Intelligent Laboratory Systems*, vol. 143, pp. 16–27, 2015.

[24] J. Zhang, "Design of a new PID controller using predictive functional control optimization for chamber pressure in a coke furnace," *ISA Transactions®*, vol. 67, pp. 208–214, 2017.

[25] H. Zou and H. Li, "Improved PI-PD control design using predictive functional optimization for temperature model of a fluidized catalytic cracking unit," *ISA Transactions®*, vol. 67, pp. 215–221, 2017.

[26] M. Xu, S. Li, and W. Cai, "Practical receding-horizon optimization control of the air handling unit in HVAC systems," *Industrial & Engineering Chemistry Research*, vol. 44, no. 8, pp. 2848–2855, 2005.

[27] K. N. Lee and Y. K. Yeo, "A new predictive PID controller for the processes with time delay," *Korean Journal of Chemical Engineering*, vol. 26, no. 5, pp. 1194–1200, 2009.

[28] H. Li, H. Zhou, and J. Zhang, "Dynamic matrix control optimization based new PIPD type control for outlet temperature in a coke furnace," *Chemometrics and Intelligent Laboratory Systems*, vol. 142, pp. 245–254, 2015.

[29] S. Wu, R. Zhang, R. Lu, and F. Gao, "Design of dynamic matrix control based PID for residual oil outlet temperature in a coke furnace," *Chemometrics and Intelligent Laboratory Systems*, vol. 134, pp. 110–117, 2014.

[30] HongboZou and H. Li, "Tuning of PI-PD controller using extended non-minimal state space model predictive control for the stabilized gasoline vapor pressure in a stabilized tower," *Chemometrics and Intelligent Laboratory Systems*, vol. 142, pp. 1–8, 2015.

[31] I. Skrjanc, "Model predictive functional control for processes with unstable poles," *Asian Journal of Control*, vol. 10, no. 4, pp. 507–513, 2008.

[32] X. Xu and M. He, "On adaptive control applied to speed regulation of marine diesel engine," in *Proceedings of the 27th Chinese Control Conference, CCC*, pp. 56–59, China, July 2008.

[33] A. Balluchi, L. Benvenuti, M. D. D. I. Benedetto, S. Member, C. Pinello, and A. Luigi, "Automotive engine control and hybrid systems: Challenges and opportunities," *Proceedings of the IEEE*, vol. 88, no. 7, pp. 888–911, 2000.

[34] E. De Santis, M. D. Di Benedetto, and G. Pola, "Digital idle speed control of automotive engines: a safety problem for hybrid systems," *Nonlinear Analysis. Theory, Methods & Applications. An International Multidisciplinary Journal*, vol. 65, no. 9, pp. 1705–1724, 2006.

[35] T. Schulze, M. Wiedemeier, and H. Schuette, "Crank angle - Based diesel engine modeling for hardware-in-the-loop applications with in-cylinder pressure sensors," *SAE Technical Papers*, 2007.

[36] S. A. Ali and S. Saraswati, "Cycle-by-cycle estimation of IMEP and peak pressure using crankshaft speed measurements," *Journal of Intelligent & Fuzzy Systems: Applications in Engineering and Technology*, vol. 28, no. 6, pp. 2761–2770, 2015.

[37] D. Dougherty and D. Cooper, "A practical multiple model adaptive strategy for single-loop MPC," *Control Engineering Practice*, vol. 11, no. 2, pp. 141–159, 2003.

[38] X. Tao, N. Li, and S. Li, "Multiple model predictive control for large envelope flight of hypersonic vehicle systems," *Information Sciences*, vol. 328, pp. 115–126, 2016.

[39] S. J. Qin and T. A. Badgwell, "A survey of industrial model predictive control technology," *Control Engineering Practice*, vol. 11, no. 7, pp. 733–764, 2003.

[40] R. Outbib, G. Graton, X. Dovifaaz, and R. Younes, "Speed control of automotive diesel engines," *International Journal of Control*, vol. 87, no. 4, pp. 812–826, 2014.

[41] T. Chamsai, P. Jirawattana, and T. Radpukdee, "Robust adaptive PID controller for a class of uncertain nonlinear systems: an application for speed tracking control of an SI engine," *Mathematical Problems in Engineering*, Article ID 510738, Art. ID 510738, 12 pages, 2015.

[42] S. Di Cairano, D. Yanakiev, A. Bemporad, I. V. Kolmanovsky, and D. Hrovat, "Model predictive idle speed control: design, analysis, and experimental evaluation," *IEEE Transactions on Control Systems Technology*, vol. 20, no. 1, pp. 84–97, 2012.

[43] D. W. Memering and P. H. Meckl, "Comparison of adaptive control techniques applied to diesel engine idle speed regulation," *Journal of Dynamic Systems, Measurement, and Control*, vol. 124, no. 4, pp. 682–688, 2002.

[44] H. Jammoussi, M. Franchek, K. Grigoriadis, and M. Books, "Closed-loop system identification based on data correlation," *Journal of Dynamic Systems, Measurement, and Control*, vol. 136, no. 1, Article ID 014507, 2014.

[45] N. N. Nandola and S. Bhartiya, "A multiple model approach for predictive control of nonlinear hybrid systems," *Journal of Process Control*, vol. 18, no. 2, pp. 131–148, 2008.

[46] M. Kang and T. Shen, "Model predictive control of gasoline engines with nonlinear feedback linearized model," in *Proceedings of the 2014 18th International Conference on System Theory, Control and Computing, ICSTCC 2014*, pp. 369–374, October 2014.

[47] O. Bondarenko and M. Kashiwagi, "Statistical consideration of propeller load fluctuation at racing condition in irregular waves," *Journal of Marine Science and Technology*, vol. 16, no. 4, pp. 402–410, 2011.

[48] S. Iqbal and A. I. Bhatti, "Load varying polytopic based robust controller design in LMI framework for a 2DOF stabilized platform," *Arabian Journal for Science and Engineering*, vol. 36, no. 2, pp. 311–327, 2011.

[49] L. Guzzella and A. Amstutz, "Control of diesel engines," *IEEE Control Systems Magazine*, vol. 18, no. 5, pp. 53–71, 1998.

[50] F. Salem and M. I. Mosaad, "A comparison between MPC and optimal PID controllers: Case studies," in *Proceedings of the Michael Faraday IET International Summit 2015*, pp. 59–65, September 2015.